Myocardial Oxygen Extraction Fraction Measured Using Bolus Inhalation of ^{15}O-Oxygen Gas and Dynamic PET

Mark Lubberink[1], Yeun Ying Wong[2], Pieter G.H.M. Raijmakers[1], Robert C. Schuit[1], Gert Luurtsema[1], Ronald Boellaard[1], Paul Knaapen[3], Anton Vonk-Noordegraaf[2], and Adriaan A. Lammertsma[1]

[1]Department of Nuclear Medicine and PET Research, VU University Medical Centre, Amsterdam, The Netherlands; [2]Department of Pulmonology, VU University Medical Centre, Amsterdam, The Netherlands; and [3]Department of Cardiology, VU University Medical Centre, Amsterdam, The Netherlands

The aim of this study was to determine the accuracy of oxygen extraction fraction (OEF) measurements using a dynamic scan protocol after bolus inhalation of $^{15}O_2$. The method of analysis was optimized by investigating potential reuse of myocardial blood flow (MBF), perfusable tissue fraction, and blood and lung spillover factors derived from separate ^{15}O-water and C^{15}O scans. **Methods:** Simulations were performed to assess the accuracy and precision of OEF for a variety of models in which different parameters from ^{15}O-water and C^{15}O scans were reused. Reproducibility was assessed in 8 patients who underwent one 10-min dynamic scan after bolus injection of 1.1 GBq of ^{15}O-water, two 10-min dynamic scans after bolus inhalation of 1.4 GBq of $^{15}O_2$, and a 6-min static scan after bolus inhalation of 0.8 GBq of C^{15}O for region-of-interest definition. **Results:** Simulations showed that accuracy and precision were lowest when all parameters were determined from the $^{15}O_2$ scan. The optimal accuracy and precision of OEF were obtained when fixing MBF, perfusable tissue fraction, and blood spillover to values derived from a ^{15}O-water scan and estimating spillover from the pulmonary gas volume using an attenuation map. Optimal accuracy and precision were confirmed in the patient study, showing an OEF test–retest variability of 13% for the whole myocardium. Correction of spillover from pulmonary gas volume requires correction of the lung time–activity curve for pulmonary blood volume, which could equally well be obtained from a ^{15}O-water rather than C^{15}O scan. **Conclusion:** Measurement of OEF is possible using bolus inhalation of $^{15}O_2$ and a dynamic scan protocol, with optimal accuracy and precision when other relevant parameters, such as MBF, are derived from an additional ^{15}O-water scan.

Key Words: PET; myocardial oxygen consumption; myocardial blood flow

J Nucl Med 2011; 52:60–66
DOI: 10.2967/jnumed.110.080408

Oxygen extraction fraction (OEF) is an important parameter in describing myocardial function (*1*). Oxygen delivery to the healthy myocardium is regulated by varying myocardial blood flow (MBF) in response to changes in oxygen demand. In diseased myocardium, however, this relationship may be disturbed, and measurement of myocardial oxygen consumption could provide additional information, because oxygen supply to the heart may also be moderated by changes in OEF.

Measurement of regional myocardial oxygen consumption has previously been described using steady-state or autoradiographic methods and applying continuous inhalation of $^{15}O_2$ oxygen gas (*1,2*). Apart from the $^{15}O_2$ scan, this protocol requires additional ^{15}O-water and C^{15}O scans to measure MBF and blood volume, respectively. Many current low-energy proton cyclotrons, however, cannot provide a steady-state delivery of $^{15}O_2$ to the patient. The availability of a bolus inhalation protocol would enable more widespread use of $^{15}O_2$ gas measurements. Such a protocol has previously been described for cerebral oxygen consumption (*3,4*), but its use for myocardial imaging has not been described and presents several additional challenges, mainly because of increased scatter and image noise and the presence of large amounts of radioactivity in the lungs during the bolus inhalation period. The measured radioactivity concentration in the myocardial wall is affected both by the limited spatial resolution of PET relative to the thickness of the myocardium and by spillover from the left- and right-ventricular cavities and the lungs. As blood volume and spillover factors can be determined directly from a dynamic ^{15}O-water scan or even from the $^{15}O_2$ scan itself, it may be possible to obtain OEF from fewer scans. Furthermore, because the total injected amount of activity in a dynamic protocol is considerably smaller than that in a steady-state protocol, a noticeable reduction in radiation burden to the patient can be achieved, especially if the C^{15}O scan can be omitted.

The aim of the present study was to establish the optimal method for analyzing dynamic PET scans after bolus inhalation of $^{15}O_2$, especially in relation to possibly reusing

Received Jun. 19, 2010; revision accepted Sep. 27, 2010.
For correspondence or reprints contact: Mark Lubberink, Department of Medical Physics and PET Centre, Uppsala University Hospital. 751 85 Uppsala, Sweden.
E-mail: mark.lubberink@akademiska.se

parameters derived from ^{15}O-water or C^{15}O scans. To this end, accuracy and precision of various OEF measures, derived from a dynamic scanning protocol, were assessed using both simulations and a test–retest study.

MATERIALS AND METHODS

Patients

Scan data from 8 patients (mean age ± SD, 45 ± 12 y) included in a clinical study on pulmonary hypertension were used in the present study. None of the patients had a documented history of cardiovascular disease. The clinical study had been approved by the Medical Ethics Review Committee of the VU University Medical Centre, and all patients gave their informed consent before inclusion in the study.

Gas Tracer Production and Administration

The gas tracer production and gas delivery system have been described in detail elsewhere (*5*). After tracer production, ^{15}O-labeled gases were collected in an empty rubber balloon within a sealed acrylic container and allowed to decay to the prescribed dose. Administration to the patient took place by forcing air into the acrylic container, which directed the ^{15}O-labeled gas from the balloon into the patient's nasal oxygen catheter (Unomedical). Previous studies have shown that approximately 20% of the measured dose in the gas delivery system is actually administered to the patient (*5*).

Scanning Procedure

Each patient underwent one 10-min dynamic emission scan after bolus injection of 1.1 GBq of ^{15}O-water, two 10-min dynamic emission scans after bolus inhalation of approximately 1.4 GBq of $^{15}O_2$, and a 6-min static emission scan starting 1 min after bolus inhalation of approximately 0.8 GBq of C^{15}O. After each scan, radioactivity was allowed to decay for 10 min before the start of the next scan. Dynamic scans consisted of 40 frames, with frame durations increasing from 5 s during the first minute to 30 s at the end of scanning. Scans were acquired on an ECAT EXACT HR+ scanner (Siemens) in 2-dimensional mode (*6*). Five blood samples were taken from the radial artery during both $^{15}O_2$ scans for measuring $^{15}O_2$ and recirculating ^{15}O-water contributions to the total blood radioactivity concentration. An additional blood sample was taken for measurement of blood oxygen content. An 80-million-count (10–15 min) transmission scan, obtained using rotating ^{68}Ge rod sources, was acquired before the ^{15}O-water scan and was used for attenuation correction of all subsequent scans. Before the C^{15}O scan, a short 5-min transmission scan was obtained to verify patient positioning. Dynamic images were reconstructed using filtered backprojection, applying a Hanning filter with a cutoff at 0.5 of the Nyquist frequency. C^{15}O images, attenuation images (μ-maps), and summed ^{15}O-water and $^{15}O_2$ images were reconstructed using ordered-subset estimation maximization with 2 iterations and 16 subsets. The summed images were used for verification of region-of-interest (ROI) positioning.

ROI Definition

For ROI definition, an anatomic tissue fraction image was calculated by subtracting the C^{15}O image, normalized to the μ-value in the left ventricle, from the corresponding μ-map (*7*). This procedure results in an image that shows only the myocardial wall (i.e., extravascular tissue). Anterior, posterior, lateral, and septal ROIs were defined on apical, basal, and mid-short-axis slices of the anatomic tissue fraction images and subsequently transferred to all other scans, which had undergone the same short-axis transformation. Similar ROIs were placed over the right-ventricular wall (RVW), which was possible because these patients had an enlarged right ventricle, with RVW thickness comparable to that of the left ventricle. ROI positioning was verified on the summed images. For both ^{15}O-water and $^{15}O_2$, a circular ROI (diameter, 1 cm) was drawn over the ascending aorta in approximately 10 consecutive image planes in the frame where the first pass of the bolus was best seen. This ROI was transferred to all dynamic frames to create an arterial whole blood time–activity curve, $C_A(t)$. In addition, an ROI was drawn in 3 image planes in the right ventricular cavity and transferred to all dynamic frames to create the right ventricular activity curve, $C_{RV}(t)$. Similarly, a large circular ROI was drawn in 3 planes in the lungs to create a lung time–activity curve, $C_L(t)$.

Input Functions

Applying a plasma–to–whole-blood ratio of 1.12 for ^{15}O-water, and with plasma containing only recirculating ^{15}O-water, we calculated the absolute $^{15}O_2$ activity concentration, $C_A^O(t)$, in blood for each of the 5 measured samples as:

$$C_A^O(t) = C_A^{wb}(t) - 1.12 \times C_A^{pl}(t). \quad \text{Eq. 1}$$

Here, $C_A^{wb}(t)$ and $C_A^{pl}(t)$ are radioactivity concentrations in whole-blood and plasma samples, respectively. Division of both sides of the equation with C_A^{wb} gives:

$$\frac{C_A^O(t)}{C_A^{wb}(t)} = 1 - 1.12 \times \frac{C_A^{pl}(t)}{C_A^{wb}(t)}. \quad \text{Eq. 2}$$

A sigmoid function was fit to the right side of Equation 2 and evaluated at all frame midpoint times. Multiplication of the measured $C_A(t)$ with this fit function yielded the $^{15}O_2$ input curve $C_A^O(t)$. The (recirculating) ^{15}O-water input curve $C_A^W(t)$ was then evaluated at all frame midpoints by fitting the solution of a 2-compartment model to the 5 measured data points $C_A^W(t)$, using a simplified version of the model suggested by Kudomi et al. (*8*), assuming a constant production rate of ^{15}O-water:

$$C_A^W(t) = \phi\, C_A^O(t) \otimes e^{-\theta t}. \quad \text{Eq. 3}$$

In Equation 3, ϕ and θ describe the average rate of conversion of $^{15}O_2$ into ^{15}O-water and the clearance rate of ^{15}O-water from blood, respectively.

Data Analysis

Myocardial Perfusion Model. Kinetics of ^{15}O-water in the heart were described by the standard single-tissue-compartment model, applying corrections for left- and right-ventricular spillover fractions V_A and V_{RV}, respectively, and for perfusable tissue fraction (PTF) α (*9,10*), which has the following solution:

$$C_{myo}^{PET}(t) = \alpha F C_A(t) \otimes e^{-\frac{F}{V_T}t} + V_A C_A(t) + V_{RV} C_{RV}(t). \quad \text{Eq. 4}$$

Here, F is MBF, and $C_{myo}^{PET}(t)$ is the radioactivity concentration in the myocardium as measured by PET.

OEF Model. The kinetics of $^{15}O_2$ in the heart can be described by:

$$\frac{dC_{myo}(t)}{dt} = EFC_A^O(t) + FC_A^W(t) - \frac{F}{V_T}C_{myo}(t). \quad \text{Eq. 5}$$

The first term on the right-hand side describes the extraction of oxygen, which is assumed to be instantaneously converted into water in the myocardium. The second term represents uptake of recirculating water and the last term clearance of water from the myocardium. Here, $C_{myo}(t)$ is the radioactivity concentration in the myocardial wall, and E is OEF. The solution of this differential equation is written as follows:

$$C_{myo}(t) = EFC_A^O(t) \otimes e^{-\frac{F}{V_T}t} + FC_A^W(t) \otimes e^{-\frac{F}{V_T}t}. \quad \text{Eq. 6}$$

In addition to spillover from the ventricles, spillover V_L from activity in the lungs $C_L(t)$ has to be considered. Furthermore, a term must be added to account for the venous blood concentration of $^{15}O_2$ due to its incomplete extraction. This results in the following total PET signal:

$$C_{myo}^{PET}(t) = \alpha EFC_A^O(t) \otimes e^{-\frac{F}{V_T}t} + \alpha FC_A^W(t) \otimes e^{-\frac{F}{V_T}t} + \alpha V_V(1 - E)C_A^O(t) + V_L C_L(t) + V_A C_A(t) + V_{RV} C_{RV}(t). \quad \text{Eq. 7}$$

In Equation 7, V_V is the venous blood volume in the myocardial wall, which has been estimated at 0.1 mL/g (*7*). If F and α are known, this equation can be solved by direct matrix inversion or by a nonnegative linear least-squares fit to prevent noise-induced negative parameter values.

Lung Spillover. As suggested previously (*1,11*), spillover from gas radioactivity in the lungs can be corrected using the μ-map to determine V_G:

$$V_G = 1 - \frac{\mu_{ROI}}{\mu_{LV}}. \quad \text{Eq. 8}$$

Because Equation 8 implicitly corrects only for spillover due to radioactivity in the gas volume in the lungs, not the total lung activity $C_L(t)$ but the time–activity curve of the gas volume $C_G(t)$ should be used in Equation 7:

$$C_G(t) = \frac{C_L(t) - V_B^L C_A(t)}{V_G^L}. \quad \text{Eq. 9}$$

Here, V_B^L and V_G^L are the fractional blood and gas volume in the lungs, respectively. The pulmonary blood volume can be determined either from the $C^{15}O$ scan:

$$V_B^L = \frac{C_L^{CO}}{C_{LV}^{CO}} \quad \text{Eq. 10}$$

or using the spillover parameters as determined in the ^{15}O-water scan. Then, the gas volume time–activity curve $C_G(t)$ is calculated as:

$$C_G(t) = \frac{C_L(t) - V_A^L C_A(t) - V_{RV}^L C_{RV}(t)}{V_G^L}. \quad \text{Eq. 11}$$

Here, V_A^L and V_{RV}^L are arterial and pulmonary circulation blood volumes, respectively, in the lungs. In both cases, instead of using V_G as based on the μ-map, V_L can be included as a fit parameter in solving Equation 7.

Parameter Estimation

Several different approaches in fitting Equation 7 to the PET data were investigated in terms of reusing parameters previously determined from ^{15}O-water or $C^{15}O$ scans (Table 1). Model 1, which is essentially the model used by Iida et al. for the steady-state method (*1*), reuses MBF and PTF from the ^{15}O-water scan and uses blood volume and gas spillover as determined from the $C^{15}O$ scan and μ-map (Eqs. 8 and 10, respectively). Models 2 and 3 reuse MBF, PTF, V_A, and V_{RV} from the ^{15}O-water scan and include V_G as determined from the μ-map, with lung blood volume based on either the $C^{15}O$ scan (Eqs. 9 and 10; model 2) or the ^{15}O-water scan (Eq. 11; model 3). Models 4 and 5 are similar to models 2 and 3, but now V_L is estimated as a fit parameter in Equation 7—that is, in the operational equation for the $^{15}O_2$ scan. Models 6 and 7 reuse MBF and PTF, or only MBF, respectively, from the ^{15}O-water scan. In model 8, all parameters were determined from the $^{15}O_2$ and $C^{15}O$ scans, applying boundaries at ±10% (F) or ±25% (α, V_A, and V_{RV}) from the results of the

TABLE 1
Parameter Estimation

Model	OEF	MBF	α	V_A	V_{RV}	V_B^L/V_L	Number*
1	$^{15}O_2$	^{15}O-water	^{15}O-water	$C^{15}O$	NA	$C^{15}O$/μ-map	1
2	$^{15}O_2$	^{15}O-water	^{15}O-water	^{15}O-water	^{15}O-water	$C^{15}O$/μ-map	1
3	$^{15}O_2$	^{15}O-water	^{15}O-water	^{15}O-water	^{15}O-water	^{15}O-water/μ-map	1
4	$^{15}O_2$	^{15}O-water	^{15}O-water	^{15}O-water	^{15}O-water	$C^{15}O/^{15}O_2$	2
5	$^{15}O_2$	^{15}O-water	^{15}O-water	^{15}O-water	^{15}O-water	^{15}O-water/$^{15}O_2$	2
6	$^{15}O_2$	^{15}O-water	^{15}O-water	$^{15}O_2$	$^{15}O_2$	^{15}O-water/$^{15}O_2$	4
7	$^{15}O_2$	^{15}O-water	$^{15}O_2$	$^{15}O_2$	$^{15}O_2$	^{15}O-water/$^{15}O_2$	5
8	$^{15}O_2$	$^{15}O_2/^{15}O$-water	$^{15}O_2/^{15}O$-water	$^{15}O_2/^{15}O$-water	$^{15}O_2/^{15}O$-water	$C^{15}O$/μ-map/$^{15}O_2$	6†
9	$^{15}O_2$	$^{15}O_2$	$^{15}O_2$	$^{15}O_2$	$^{15}O_2$	$C^{15}O$/μ-map	5

*Number of parameters to be estimated from $^{15}O_2$ scan.
†5 parameters estimated within limits from results of ^{15}O-water scan.
NA = not applicable.

^{15}O-water scan. This application of boundaries would allow for compensation for inaccurate ROI placement due to small patient movements between scans or for small physiologic changes between scans. In model 9, all parameters were determined from the $^{15}O_2$ and C^{15}O scans without any information from the ^{15}O-water scan.

Model 9 would allow measurement of all parameters without an additional ^{15}O-water scan, whereas models 3 and 5 would obviate an additional C^{15}O scan. For models 8 and 9, parameters were estimated using nonlinear regression of Equation 7. In approaches 1–7, which are essentially linear problems because MBF is reused from the results of the ^{15}O-water scan, parameters were estimated using nonnegative least squares. All linear models were evaluated with (models 1–7) and without (models 1′–7′) accounting for venous $^{15}O_2$ due to incomplete extraction of $^{15}O_2$. Only a limited number of these models, chosen on the basis of the results of the simulation study, was used for analysis of patient data.

Simulations

^{15}O-water and $^{15}O_2$ time–activity curves (n = 1,000) were calculated according to Equations 4 and 7, with randomly chosen parameters $0.3 < MBF < 5$ mL·g^{-1}·min^{-1}, $0.3 < OEF < 1$, $0.1 < V_A < 0.3$, and $0.1 < V_{RV} < 0.3$ or $V_{RV} = 0$, $0.3 < PTF < 1.0$, and $0.15 < V_L < 0.25$. For each ^{15}O-water and $^{15}O_2$ time–activity curve generated, normally distributed noise was added corresponding to typical noise levels found in segmental time–activity curves in patients (average SD, 10% and 20% in the last 20 frames for ^{15}O-water and $^{15}O_2$, respectively). Parameters used for generating ^{15}O-water and $^{15}O_2$ time–activity curves either were identical—assuming both no physiologic changes between scans and no patient movements—or were varied, with randomly distributed changes with an SD of 5% (F, PTF) or 10% (V_A, V_{RV}, and V_L). Simulated time–activity curves were analyzed according to the approaches described in the sections above, and correlation and agreement between true and simulated OEF were addressed using linear regression and Bland–Altman plots (*12*). In addition, accuracy and precision of OEF for typical parameter values found in the left ventricular wall (LVW) and RVW and septum were estimated using simulations of 100 noisy time–activity curves with MBF = 1, OEF = 0.6, V_A = 0.25, V_L = 0.2, and V_{RV} = 0.15 or 0 or MBF = 0.5, OEF = 0.6, V_A = 0.1, V_{RV} = 0.2, and V_L = 0.2, respectively.

Test–Retest Study

The level of agreement between test and retest values was assessed using the intraclass correlation coefficient with a 2-way random model with absolute agreement. In addition, Bland–Altman analysis was used, plotting the percentage difference between 2 measured values against the mean of both. Systematic bias and a possible dependency of agreement on absolute values of extraction fraction were assessed by linear regression. Additionally, the repeatability coefficient was calculated as the SD of the mean relative difference between test and retest OEF values.

RESULTS

Figure 1 shows $C_A^O(t)/C_A^{wb}(t)$, the fit used to determine the $^{15}O_2$ input curve, and the compartment model fit used to estimate the ^{15}O-water water input curve for a typical patient during inhalation of $^{15}O_2$. Clearly, the compartment model of Equation 3 gave a good description of the measured activity concentrations of ^{15}O-water.

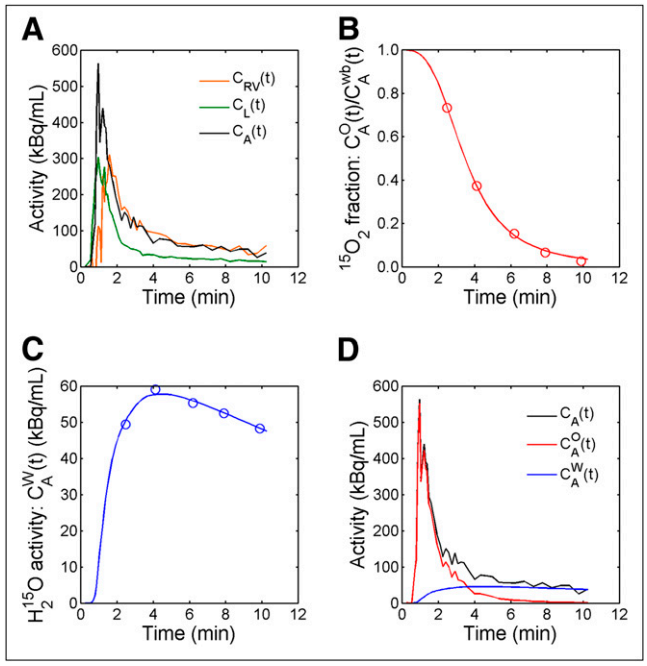

FIGURE 1. Ascending aorta, right ventricle, and lung time–activity curves (A), ratio of $^{15}O_2$ to whole-blood concentrations (B), compartment model fit of ^{15}O-water radioactivity concentration in blood (C), and resulting $^{15}O_2$ and ^{15}O-water input functions (D) for typical patient during $^{15}O_2$ inhalation.

Results of the simulations are shown in Figure 2 and Supplemental Figures 1 and 2 (supplemental materials are available online only at http://jnm.snmjournals.org). In the simulations, both models 2 and 3 and models 4 and 5 were indistinguishable from each other because no C^{15}O scan was simulated and identical lung blood volumes were used. Therefore, only values for models 2 and 4 are reported. Clearly, reuse of parameters from the ^{15}O-water scan led to more robust values of OEF, whereas determining all parameters from the $^{15}O_2$ scans gave the least robust results, as seen in Figure 2. As shown in Figure 2 and Supplemental Figure 1, omission of a correction for venous $^{15}O_2$ (due to limited extraction of $^{15}O_2$) in models 2′, 3′, and 4′ leads to a positive bias in OEF. This bias is inversely proportional to OEF itself, increasing to around 25% for OEF values of 0.3, and therefore these models were excluded from further evaluation. Furthermore, as shown in Supplemental Figure 2, the impact of movements or small physiologic changes on the accuracy of OEF measurements is still smaller for model 2 (and models 3–5, data not shown), which reuses parameters from the ^{15}O-water scan, than for model 8, which allows for some variation of these parameters. Models 2 and 4, which differ only in the way of determining lung spillover (from μ-map or as fit parameter, respectively), performed equally well in the simulation study.

On the basis of the results of the simulations, only models 1–5 were used for analysis of patient data, all including a correction for noncomplete extraction of $^{15}O_2$. Figure 3 shows test–retest variability of OEF values using

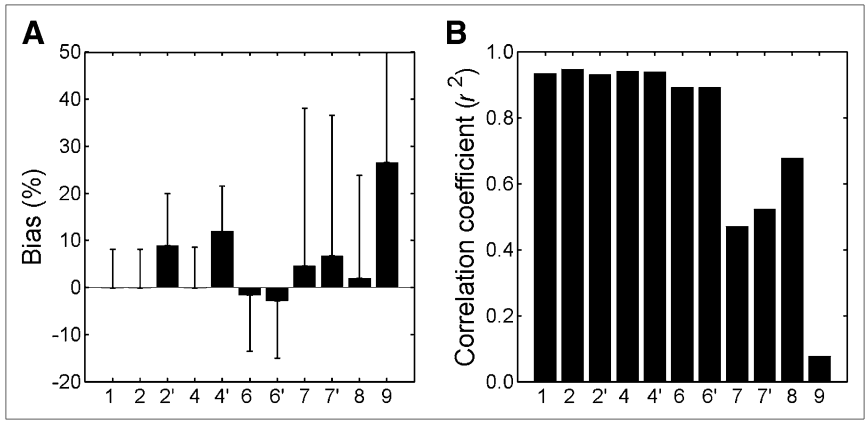

FIGURE 2. Simulation study: mean bias (± SD) of fitted OEF relative to true (simulated) OEF (A) and correlation coefficient (r^2; B) between fitted and true values for all models.

these 5 models. Intraclass correlation coefficients are given in Table 2. The best reproducibility was found for models 2 and 3, which reuse MBF, PTF, V_A, and V_{RV} from the ^{15}O-water scan and use a lung spillover factor determined from the μ-map. Variability in OEF determined using models 4 or 5, which include V_L as a fit parameter, was slightly larger than for models 2 or 3, especially in the LVW. Correlation and Bland–Altman plots of model 3 are shown in Figure 4.

The mean test–retest variability for individual myocardial segments was 27% using models 2 and 3, compared with 13% for the whole myocardium. The repeatability coefficient for the whole myocardium was 29% using models 2 and 3. Figure 5 shows mean OEF values, obtained with models 1–5, for the present patient population.

DISCUSSION

The present study describes a method for measuring OEF using dynamic PET scans after bolus inhalation of $^{15}O_2$. Reusing MBF, PTF, and blood spillover fractions estimated from an additional ^{15}O-water scan, with lung spillover estimated using a μ-map, yielded optimal precision and accuracy, with a test–retest variability of 13% and a repeatability coefficient of 29% for whole myocardium and slightly larger values for left- and right-ventricular free walls and septum. These values cannot be compared with steady-state OEF values, because no test–retest studies in patients have been reported for this method. Although the present variability is larger than the reported repeatability coefficient values of around 20% for ^{15}O-water tumor perfusion measurements (*13*) or proliferation measurements using ^{18}F-FLT (*14*), it is acceptable for intergroup comparisons. On a myocardial segment basis, however, test–retest variability increases to 27%. Moreover, in many cases model fits of single segments resulted in physiologically meaningless values of OEF greater than 1 or OEF close to 0. Therefore, measurement of OEF using the present method is limited to larger ROIs such as the whole LVW or RVW or septum. On the other hand, if with the latest-generation PET/CT scanners an improvement in $^{15}O_2$ image quality similar to that for ^{15}O-water can be achieved (*15*), improved quantification in individual myocardial segments may become feasible using these newer PET systems, possibly even based on only a single $^{15}O_2$ scan. A limitation of the present work is that it is based on a small patient group. There is a need for larger studies in different patient populations to confirm the presented results, ideally in comparison to the steady-state method.

There were no significant differences in OEF values between the various methods, except for model 1 (Fig. 5). Model 1 provided much lower OEF values than did the other models. Mean (±SD) values of OEF in the left ventricle and septum for models 2–4 (0.66 ± 0.12 and 0.68 ± 0.11 for models 2 and 3, respectively) were not significantly different from those reported previously (0.60 ± 0.11) for healthy volunteers using the steady-state method (*1*). Because the results of the steady-state method corresponded well with invasive measurements (*2*), and possibly a slightly higher OEF could be expected in the present patient group, the lower OEF results of model 1 (0.51 ± 0.23) are physiologically not plausible. The much larger

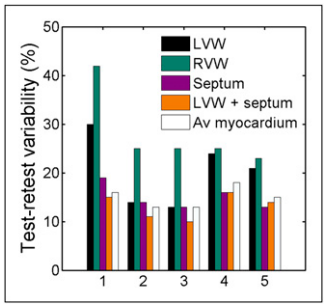

FIGURE 3. Clinical study: average test–retest variability of OEF using models 1–5. Av myocardium = average myocardium.

TABLE 2
Intraclass Correlation Coefficients

ROI	Model 1	2	3	4	5
Average myocardium	0.96	0.75	0.70	0.68	0.66
LVW plus septum	0.76	0.85	0.84	0.84	0.72
LVW	0.99	0.75	0.80	0.71	0.14
RVW	0.63	0.54	0.57	0.54	0.58
Septum	0.87	0.70	0.72	0.78	0.81

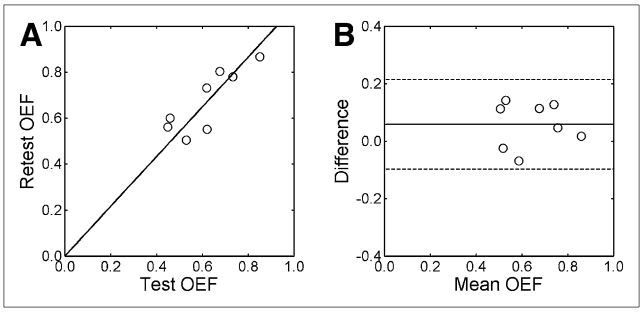

FIGURE 4. Clinical study: correlation (A) and Bland–Altman (B) plots of OEF determined using model 3 for LVW.

range of OEF values found with model 1 also explains the high intraclass correlation coefficients for this model, which erroneously suggest good reproducibility. Probably, even small differences in ROI positioning between $C^{15}O$ and $^{15}O_2$ scans cause large errors in patient studies when using this method.

Methods that fit for lung spillover V_L show poorer reproducibility than methods that use a lung spillover factor determined from the μ-map. Models 6 and 7, which also include blood spillover as fit parameter, showed poor accuracy (Fig. 2) in the simulations and were not evaluated in the clinical study. The similar shape of the lung, arterial blood, and right-ventricular time–activity curves, as clearly shown in Figure 1A, along with the relatively high noise level of myocardial time–activity curves, makes them effectively indistinguishable in the fit procedure, which also affects the accuracy and precision of the other parameters.

Model 3 allows for measurements of OEF based only on $^{15}O_2$ and ^{15}O-water scans, obviating an additional $C^{15}O$ scan. In the present study, the $C^{15}O$ images were used to create an anatomic tissue fraction image on which ROIs were defined. In principle, parametric MBF or PTF images could be used for ROI definition instead. Although it was not possible to construct parametric MBF and PTF images of sufficient image quality using the 2-dimensional PET data in the present study, state-of-the-art PET/CT scanners with much improved scan statistics do allow for generation of good-quality parametric images and $C^{15}O$ scans will no longer be needed for delineation of myocardial segments (*15,16*). Apart from increasing patient comfort because of the shorter duration of the total procedure, this method also decreases the possibility of errors due to patient movement between the different scans. In addition, the major part of the total radiation dose is due to the $C^{15}O$ scan. Although the availability of OEF measurements using PET may be expanded using the current method because it avoids the need for a $C^{15}O$ scan, uses a standard PET cyclotron, and results in reduced radiation dose, feasibility of routine clinical use is dependent on improved automation of data analysis and the availability of a gas administration system.

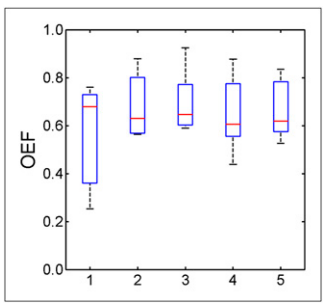

FIGURE 5. Clinical study: whole-myocardium OEF values in patients as determined using models 1–5.

The total effective dose to the patient in a continuous infusion–inhalation protocol consisting of ^{15}O-water, $^{15}O_2$, and $C^{15}O$ scans has been reported to be 10.5 mSv (*1*). Omitting the $C^{15}O$ scan and using bolus administrations of ^{15}O-water (1.1 GBq) and $^{15}O_2$ (1.4 GBq), followed by dynamic scanning, lead to a considerable reduction in effective dose (to ~2 mSv). Absorbed doses could be reduced further with the latest-generation PET/CT scanners because of the possibility of using smaller amounts of radioactivity (*15*).

CONCLUSION

Measurement of OEF is possible using a dynamic scan protocol after bolus inhalation of $^{15}O_2$ when MBF, PTF, and blood spillover factors are derived from an additional ^{15}O-water scan and spillover from pulmonary gas volume is estimated from an attenuation map, with correction for pulmonary blood volume based on the ^{15}O-water scan. Omission of a $C^{15}O$ blood volume scan reduces the risk of errors due to patient movement between scans. The proposed method, compared with a continuous infusion–inhalation protocol, results in a significant reduction in radiation burden to the patient and leads to improved feasibility of oxygen consumption measurements using $^{15}O_2$ and PET.

ACKNOWLEDGMENTS

We thank Suzette van Balen and Femke Jongsma for performing the scans and Kevin Takkenkamp and Henri Greuter for producing ^{15}O-labeled tracers.

REFERENCES

1. Iida H, Rhodes CG, Araujo LI, et al. Noninvasive quantification of regional myocardial metabolic rate for oxygen by use of $^{15}O_2$ inhalation and positron emission tomography: theory, error analysis, and application in humans. *Circulation.* 1996;94:792–807.
2. Yamamoto Y, de Silva R, Rhodes CG, et al. Noninvasive quantification of regional myocardial metabolic rate of oxygen by $^{15}O_2$ inhalation and positron emission tomography: experimental validation. *Circulation.* 1996;94:808–816.
3. Rijbroek A, Boellaard R, Vriens EM, Lammertsma AA, Rauwerda JA. Peroperative neuromonitoring during carotid endarterectomy in relation to preoperative positron emission tomography findings. *Eur J Vasc Endovasc Surg.* 2008;35:652–660.
4. Holden JE, Eriksson L, Roland PE, Stone-Elander S, Widen L, Kesselberg M. Direct comparison of single-scan autoradiographic with multiple-scan least-squares fitting approaches to PET $CMRO_2$ estimation. *J Cereb Blood Flow Metab.* 1988;8:671–680.
5. Luurtsema G, Boellaard R, Greuter HN, et al. Pharmaceutical preparation of oxygen-15 labelled molecular oxygen and carbon monoxide gasses in a hospital setting. *J Clin Pharm Ther.* 2010;35:63–69.
6. Brix G, Zaers J, Adam LE, et al. Performance evaluation of a whole-body PET scanner using the NEMA protocol. *J Nucl Med.* 1997;38:1614–1623.
7. Iida H, Rhodes CG, de Silva R, et al. Myocardial tissue fraction–correction for partial volume effects and measure of tissue viability. *J Nucl Med.* 1991;32:2169–2175.

8. Kudomi N, Hayashi T, Watabe H, et al. A physiologic model for recirculation water correction in $CMRO_2$ assessment with $^{15}O_2$ inhalation PET. *J Cereb Blood Flow Metab.* 2009;29:355–364.
9. Hermansen F, Rosen SD, Fath-Ordoubadi F, et al. Measurement of myocardial blood flow with oxygen-15 labelled water: comparison of different administration protocols. *Eur J Nucl Med.* 1998;25:751–759.
10. Iida H, Kanno I, Takahashi A, et al. Measurement of absolute myocardial blood flow with $H_2{}^{15}O$ and dynamic positron-emission tomography: strategy for quantification in relation to the partial-volume effect. *Circulation.* 1988;78:104–115.
11. Valind SO, Rhodes CG, Brudin LH, Jones T. Measurements of regional ventilation pulmonary gas volume: theory and error analysis with special reference to positron emission tomography. *J Nucl Med.* 1991;32:1937–1944.
12. Bland JM, Altman DG. Statistical methods for assessing agreement between two methods of clinical measurement. *Lancet.* 1986;1:307–310.
13. de Langen AJ, Lubberink M, Boellaard R, et al. Reproducibility of tumor perfusion measurements using ^{15}O-labeled water and PET. *J Nucl Med.* 2008;49:1763–1768.
14. de Langen AJ, Klabbers B, Lubberink M, et al. Reproducibility of quantitative ^{18}F-3′-deoxy-3′-fluorothymidine measurements using positron emission tomography. *Eur J Nucl Med Mol Imaging.* 2009;36:389–395.
15. Van der Veldt AA, Hendrikse NG, Harms HJ, et al. Quantitative parametric perfusion images using ^{15}O-labeled water and a clinical PET/CT scanner: test-retest variability in lung cancer. *J Nucl Med.* 2010;51:1684–1690.
16. Knaapen P, de HS, Hoekstra OS et al. Cardiac PET-CT: advanced hybrid imaging for the detection of coronary artery disease. *Neth Heart J.* 2010;18:90–98.

The Journal of NUCLEAR MEDICINE

Myocardial Oxygen Extraction Fraction Measured Using Bolus Inhalation of ^{15}O-Oxygen Gas and Dynamic PET

Mark Lubberink, Yeun Ying Wong, Pieter G.H.M. Raijmakers, Robert C. Schuit, Gert Luurtsema, Ronald Boellaard, Paul Knaapen, Anton Vonk-Noordegraaf and Adriaan A. Lammertsma

J Nucl Med. 2011;52:60-66.
Published online: December 13, 2010.
Doi: 10.2967/jnumed.110.080408

The Journal of Nuclear Medicine is published monthly.
SNMMI | Society of Nuclear Medicine and Molecular Imaging
1850 Samuel Morse Drive, Reston, VA 20190.
(Print ISSN: 0161-5505, Online ISSN: 2159-662X)

SNMMI SOCIETY OF NUCLEAR MEDICINE AND MOLECULAR IMAGING